Full paper

Mie-resonant mesoporous electron transport layer for highly efficient perovskite solar cells

Aleksandra Furasova [a,b,*], Pavel Voroshilov [a], Mikhail Baranov [a], Pavel Tonkaev [a], Anna Nikolaeva [a], Kirill Voronin [a], Luigi Vesce [b], Sergey Makarov [a,**], Aldo Di Carlo [b,**]

[a] The Department of Physics and Engineering ITMO University, Saint-Petersburg, Russia
[b] C.H.O.S.E. (Centre for Hybrid and Organic Solar Energy), Department of Electronic Engineering, University of Rome-Tor Vergata, Rome, Italy

ARTICLE INFO

ABSTRACT

All-dielectric nanophotonics is a powerful tool for improvement of thin-film optoelectronic devices because of low optical losses, strong light localization, and chemical robustness against such materials as halide perovskites. However, large-scale and low-cost approaches to create functional nanostructures are still not developed. In our work, we show a novel method to create mesoporous electron transport layer based on optically resonant silicon nanoparticles incorporated into TiO_2 paste to be applied for perovskite ($MAPbI_3$) solar cell. The inclusion of Mie-resonant silicon nanoparticles helps to improve light absorption by a perovskite layer without reduction of the active material. The management of Si nanoantennas concentration provides to reach a power conversion efficiency higher than 21% by increasing all main device parameters. Our multi-physical theoretical simulations of the solar cells with the resonant silicon nanoparticles provide physical understanding on the mechanisms of the device improvement as well as help to optimize the silicon nanoparticles concentration.

1. Introduction

Recent progress in nanophotonic designs for thin-film photovoltaics is attributed to the ability of optically resonant nanostructures to improve light control and light trapping by photovoltaic active materials, which is the crucial for thin-film device technology [1–4]. Plasmonic nanoparticles (NPs) represent a majority of photonic nanostructures for perovskite solar cells (PSCs) [5–7]. However, plasmonic nanostructures made of gold or silver possess high dissipative losses in visible range due to their negative real part of dielectric permittivity, and non-negligible value of the imaginary part, that is common for all metals. Also, to avoid chemical reaction of metal NPs with high surface energy it is necessary to coat them by additional dielectric spacer [8–10].

On the other hand, all-dielectric nanoparticles with high refractive index (RI) can be more prospective for photovoltaic technology due to broad spectral tunability of their optical resonances, strong light scattering, and enhancement of optical near-field [11]. The interplay between magnetic and electric multipoles in the dielectric NPs at the same wavelengths leads to resonant control of scattering efficiency and directionality [12]. Moreover, in contrast to the plasmonic nanostructures, high-index dielectric NPs have a positive value

of dielectric permittivity with low imaginary part reducing dissipative losses and parasitic absorption [11], which is crucial for photovoltaic applications [1].

One of the most rapidly developing families of materials for optoelectronics and photovoltaics is lead halide perovskites [13–16], where carrier management [17] and photon management [18] are two main directions of the devices performance optimization. Despite the high potential of the all-dielectric platform for both carrier and photon managements [19,20], its fabrication methods are still time-consuming and expensive [21], which prevents their usage to develop high-efficient and large-scale optoelectronic devices.

In this work, we overcome this limitation by developing a novel method to create TiO_2 mesoporous electron transport layer (ETL) with commercial optically resonant silicon NPs. The created paste is demonstrated to be one of the best candidates for perovskite solar cells improvement among those with integrated resonant NPs. Namely, an optimized concentration of Si nanoantennas inside the paste allows to reach a power conversion efficiency >21% via the improvement of light absorption in a $MAPbI_3$ based perovskite layer without reduction of the

Fig. 1. (a) Schematic illustration of prepared perovskite solar cell with 100–200 nm in a diameter Mie resonant nanoantennas. (b) Experimental dark-field spectra of Si NPs located on the surface of mesoporous TiO_2 layer (SEM images are given in with scale bars 200 nm.) measured for scattered s-polarized incident light (angle of incidence is 65°) and (c) corresponding calculated scattering efficiency spectra for Si NPs with the similar size.

active material, which is confirmed by our multi-physical theoretical simulations.

2. Results and discussion

Crystalline silicon NPs have RI number $n \approx 4$ that allows to support strong Mie resonances even in the materials used for PSCs, i.e. with $n \approx 2$ and absorption level in the PSC's operation spectrum much lower than that of metals. In order to confirm that experimentally, we provide polarization-resolved scattering spectral measurements using the s-polarized light from a halogen lamp at an angle of 65° (for details, see Experimental section). Fig. 1b shows the scattering spectra of agglomerated Si NPs from the mesoporous layer (Fig.S1,S2). These clusters of NPs can be considered as the individual particles with larger size of about 500–600 nm and produce strong scattering signal being the result of high electric and magnetic modes contributions (Fig. 1c). It is worth noting that the formed quasi-spherical clusters can scatter the incident light as NPs with larger size and can support high-order modes such as electric quadrupole (EQ), electric octupole (EO) and electric hexadecapole (EH) and magnetic quadrupole (MQ), magnetic octupole (MO), magnetic hexadecapole (MH) as shown in Fig. S3. For NPs with size less than 200 nm electric and magnetic dipoles (MD, ED) and quadrupoles contribute mostly. It worth noting that we also collect the Rayleigh scattering signal from the mesoporous layer consisting of 20-nm TiO_2 NPs that can significantly increase the signal in a blue spectral range. Nevertheless, Mie scattering from Si NPs is much stronger, which is confirmed by dark-field optical images of the mesoporous layer with Si NPs (Fig. S2) with a size about 100–200 nm. The existence of the electric and magnetic types of Mie modes in the studied Si NPs is confirmed by our full-wave electromagnetic simulations in Comsol Multiphysics. The scattering geometry is modeled as a crystalline Si spherical particle partly plunged in TiO_2 substrate. The particle is irradiated by a plane wave at an angle of 65° in air. Modeling of scattering spectra (Fig. 1c) shows good agreement with the corresponding experimental ones. Some difference between the shapes of theoretical and experimental spectra arise from the mesoporous structure of the substrate and non-spherical shape of the considered clusters.

Fig. 2a shows a colored cross-section scanning electron microscopy (SEM) image of the completed PSC device including resonant NPs in mesoporous TiO_2 layer. To create devices with different concentrations of Si NPs, we add them in the mesoporous layer by mixing solution of Si NPs and TiO_2 paste in five proportions, and the resulting pastes are shown in Fig. 2b. More details on the preparation of the mesoporous layer with Si NPs are given in Experimental Section in detail.

There are two main advantages of incorporation of Si NPs exactly into the mesoporous layer. On the one hand, the mesoporous layer can accommodate more NPs than any other layer without significant substitution of perovskite and, thus, do not change the active volume

for charge carriers photogeneration. At the same time, strongly scattering NPs should be in front of the perovskite layer relatively to the incident light to increase their contribution to the light absorption by the photoactive material [22].

Fig. 2c–g shows SEM top views of the mesoporous layers prepared from TiO_2 solutions with different Si NPs concentrations. According to the mass relations between Si and TiO_2 NPs in the mesoporous layer, one can estimate the characteristic distance between Si NPs in the volume of the mesoporous layer. For the small concentration (solution №2, Fig. 2b), it is 300–500 nm. For the optimal case (solution №3, Fig. 2b) the distance is 240–350 nm. For the high Si concentration (solution №4, Fig. 2b), the distance is 190–230 nm, and for extra high Si concentration (solution №5, Fig. 2b) the distance is 160–200 nm. According to the obtained SEM images (Fig. 2c–g), the mesoporous layers at small and optimal concentrations of Si NPs have very low density of Si NPs clusters, which are lying on the surfaces. At the same time, the average distance between Si surface agglomerates is 4.4 μm, corresponding to their concentration up to 5% that is much less than the estimated concentration of individual Si NPs inside the mesoporous layer and their influence can be ignored.The SEM images (Fig.S4) show that the perovskite films have similar morphology and does not depend on the concentration of Si NPs in mesoporous ETL. The presence of crystalline Si NPs is also confirmed by XRD measurements (Fig. S5), where the peak intensity of c-Si increases with the growth of Si NPs concentration inside the mesoporous layer. Additionally, the provided time-resolved photoluminescence (PL) measurements (Fig.S6) reveal the Si NPs influence on perovskite film properties. We fit the obtained PL signal decay data according to ABC model [23]: $-\frac{dn}{dt} = A \cdot n + B \cdot n^2 + C \cdot n^3$, where A is a monomolecular nonradiative constant, B is a bimolecular radiative constant, and C is Auger recombination which is observable in the obtained PL decay curves. While the B stays the same for all obtained decay curves, A slightly goes down with Si NPs concentration growth and keeps stable from the optimal Si NPs concentration. This tendency reveals the better crystallization quality of the perovskite films in presence of Si NPs correlating with the previous studies [24].

The scattering effect from high-index NPs implies the light concentration by a photoactive material and enhancing of light trapping [25]. Fig. S6a,b shows the PL spectra from the perovskite layer located on the mesoporous substrates with different concentration of Si NPs. The maximum PL peak intensity corresponds to the sample with the optimal concentration of Si NPs in the mesoporous layer that is the indicator of efficient light tapping [22,26]. At the higher concentrations of Si NPs, the perovskite PL signal starts to decrease, because the screening of incident UV light from the mercury lamp (for details, see Experimental Section) in the mesoporous layer and less energy penetrates into the perovskite. This effect correlates with our absorption measurements in the whole visible range, where Si NPs improves light absorption in the perovskite layer (Fig. S7).
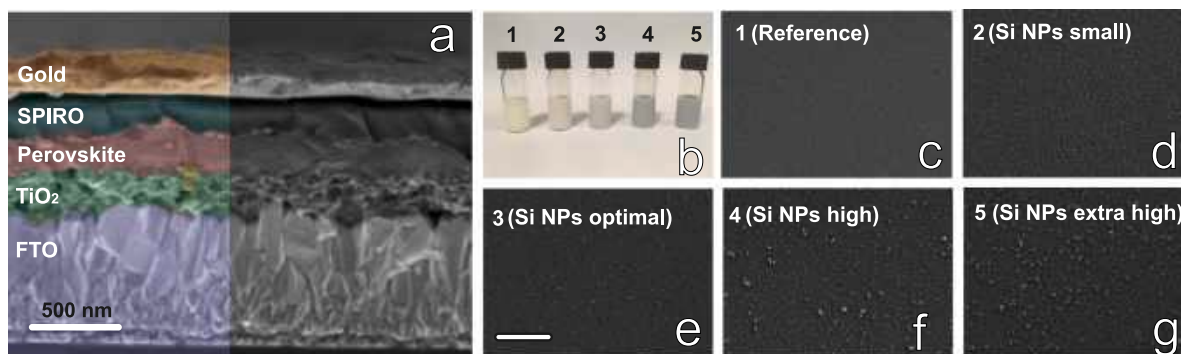
Fig. 2. (a) SEM image of the perovskite solar cell cross-section. (b) TiO$_2$ paste solution with different concentrations of Si NPs for further deposition mesoporous electron transport layer. SEM image of the prepared mesoporous layer from TiO$_2$ solutions containing different concentrations of Si NPs: (c) reference cell without Si NPs, (d) mesoporous layer with 'small' concentration of Si NPs (1:180 in mass concentrations), (e) mesoporous layer with 'optimal' concentration of Si NPs (1:120), (f) mesoporous layer with 'high' concentration of Si NPs (1:60), and (g) mesoporous layer with 'extra high' concentration of Si NPs (1:30).

To test the proposed nanophotonic approach based on Mie resonant Si NPs theoretically and experimentally for perovskite photovoltaics, we employ *n-i-p* solar cell structure representing the following architecture: FTO/compact TiO$_2$/mesoporous TiO$_2$/MAPbI$_3$/SPIRO-MeOTAD/ Au, which is one of the most commonly used for PSCs [27–31] with well known physical properties [32–36].

First of all, in order to understand the physical processes occurring in the presence of Si NPs in PSCs, it is important to investigate theoretically the influence of Si NPs located in mesoporous ETL on the charge collection efficiency. In our qualitative analysis (see details on the cells calculation in Experimental Section), we study the two following cases: Si NP in direct contact with the perovskite layer (Fig. 3a) and Si NP isolated from the perovskite by a thin TiO$_2$ covering layer (Fig. 3b) similarly to the experimental architecture in our devices. Generally, Si is a narrow band gap material as compared to MAPbI$_3$, resulting in charge carriers losses after its usage in PCSs. First of all, its contact with the active layer may lead to undesirable carrier losses in the bulk of NP attributed to parasitic recombination of electrons and holes from the active layer in the absence of energy barrier for both types of charges. In other words, crystalline Si NP serves as a recombination center that decrease the electrical performance of the device. This statement is confirmed by the energy band diagram calculated for Si NP being in contact with the active layer (Fig. 3a.1). The quasi-Fermi level for holes is bent up near the surface of NP, and the net recombination rate distribution has high values (i.e. of the same order as the generation rate, see Fig. 3a.2 and Fig. 3a.3) in the Si region. However, these losses can be efficiently suppressed by a thin TiO$_2$ protective coating around the surface of Si NP which prevents direct contact of perovskite and NP (see Fig. 3b.2 and Fig. 3b.3). In this case, TiO$_2$ creates a required barrier for holes which does not allow them to fall into Si bulk. Note, that in both cases Si contribute to charge collection attracting electrons at the distance approximately half of NPs' radius as follows from Fig. 3a.4 and Fig. 3b.4.

To deeper investigate the influence of Si NP concentration on the charge collection efficiency, we calculated open-circuit voltage V$_{OC}$ as a function of the distance between neighbor particles for both covered and uncovered cases. In our model, we assume that Shockley–Read–Hall recombination in the perovskite layer is suppressed by the inclusion of Si NPs which is confirmed by the time-resolved PL measurements (Fig. S6). First, we considered the covered case (Si NP isolated from the active region by a thin TiO$_2$ covering layer) and fixed the period near the optimal value 300 nm to find the relative change of V$_{OC}$ depending on carrier lifetime. The behavior of the blue curve in Fig. S8 confirms that the improved V$_{OC}$ characteristics of samples with Si NPs can be attributed to the extended carrier lifetime in the perovskite layer. Next, we fixed the carrier lifetime corresponding to the optimal concentration and varied the period of the unit cell containing covered Si NP. As shown in Fig.S8, V$_{OC}$ slightly improves with the period

and the curve becomes almost flat at the values higher than 400 nm. The relative increase here (around 1%–2%) is dictated mostly by the reduced defect density and better crystallization of the perovskite layer. This situation corresponds to low and moderate concentrations of Si NPs when the most of NPs are located within the mesoporous layer leading to the increased roughness of TiO$_2$ as can be seen from SEM images in Fig. 2d–e. At the higher concentrations, a number of Si agglomerates is formed on the surface of TiO$_2$ which are not protected from the contact with the perovskite layer (Fig. 2f–g). As a result, charge collection dramatically drops due to recombination losses described above. The density of uncovered Si NPs strongly affects V$_{OC}$ value which decreases by more than 5% at periods smaller than 1 μm (see Fig.S8).

The photovoltaic (PV) performances of the mesoporous layers with different concentration of Si NPs are tested for a standard *n-i-p* architecture of PSCs (see details on the cells fabrication in Experimental Section) upon irradiation of PSCs are given in Table 1. J–V curves, external quantum efficiencies, EQE (Fig. S9), and statistical numbers for efficiency, short-circuit current (J$_{SC}$), open-circuit voltage (V$_{OC}$), and fill factor (FF) a solar simulator with AM 1.5G class A spectrum. The best (Fig. 4a,b) and average Fig. 4c–f values for main PV parameters are studied. The reference device with the highest efficiency of 18% possesses an open-circuit voltage of V$_{OC}$=1.011 V, a short-circuit density of J$_{SC}$=21.8 mA/cm^2, and FF=81.5% under reverse bias that corresponds to one of the best results among all MAPbI$_3$-based PSCs.

Fig. 4b shows the comparison of EQE between the reference cell with the best efficiency and devices with different density of Si NPs in the mesoporous layer that also demonstrates the role of Mie resonant NPs on the photocurrent performance while they are located in PSCs in various concentrations. For the optimal case, EQE is clearly increased almost in the whole operating range for MAPbI$_3$ perovskite, correlating with the absorption spectra (Fig. S7). At extra high Si NPs concentration, the EQE performance is lower than for the reference PSC only in 600–660 nm range but the collected EQE photocurrent (Fig. S9b) remains to be higher for all cases with Si NPs. The total current density curves obtained from EQE mapped to J$_{SC}$ from J–V curves that is proved for the best cells and for the average J$_{SC}$ numbers.

As shown in Table 1, the inclusion of Si NPs into the mesoporous layer increases the efficiency up to 21.1% at the carefully selected concentration of them. At the optimal Si NPs concentration, the best cell has the following parameters: V$_{OC}$ = 1.036 V, J$_{SC}$ = 23.8 mA/cm^2, and FF = 85.7% under reverse voltage scan. Further, at the high Si NPs concentration the best efficiency is 18.6% with V$_{OC}$ = 1.014 V, J$_{SC}$ = 24.2 mA/cm^2, and FF = 75.8% that is still higher than for the reference. Finally, at extra high Si NPs concentration in the mesoporous layer, the PV performance starts to decrease because the average distance between centers of individual NPs reduces to ~230–160 nm.
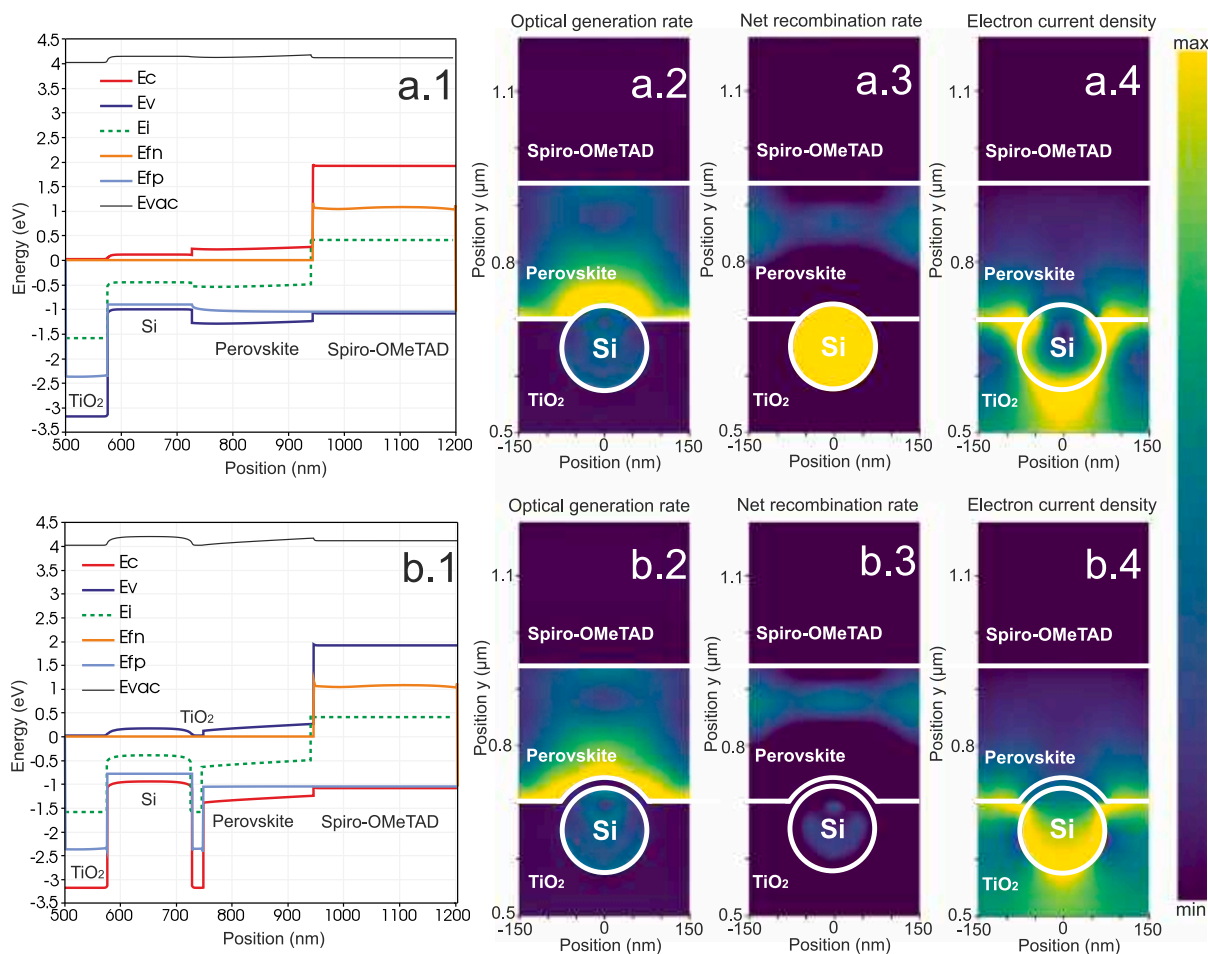
Fig. 3. Energy band diagrams, optical generation rate, net recombination rate and electron current density at V = Voc for Si NP partially submerged in perovskite in the following two cases: Si NP in direct contact with perovskite layer (a) and Si NP isolated from perovskite by a thin TiO₂ covering (b).
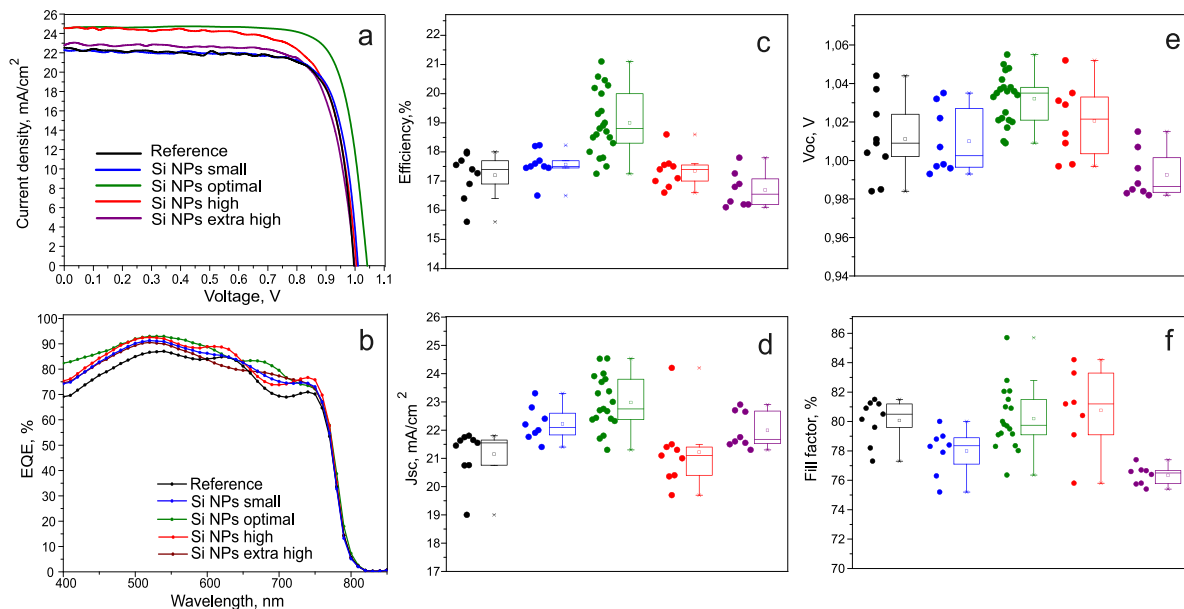

Fig. 4. (a) J–V curves for mesoporous PSCs recorded under the forward scan and containing Si NPs with different concentration: black dot line — without Si, blue — in small concentration (1:180 in mass concentrations), green — Si NPs in the optimal concentration (1:120), red — device with high Si concentration (1:60), purple — the extra high Si concentration (1:30). J–V curves and PV parameters obtained under reverse and forward bias are shown in Fig. S12. (b) External quantum efficiency for PSCs with different concentration of Si NPs inside the mesoporous layer. The statistical parameters obtained from all measured mesosilicon-based devices: (c) resulting efficiency, (d) short-circuit current, (e) open-circuit voltage, (f) filling factor.

Table 1

Best and average values of efficiency, V_{OC}, J_{SC}, and FF for the PSCs with different concentration of Si NPs inside the mesoporous layer recorded under 1 sun illumination intensity at a reverse bias. The J–V parameters at forward and reverse scans for each kind of the best cells are presented in fig.S12.

	Efficiency, % (best/average)	Voc, V (best/average)	Jsc (best/average)	FF, % (best/average)
Reference	18/17.2	1.011/1.011	21.8/21.2	81.5/80.2
Si NPs small	18.2/17.5	1.035/1.010	22/22.3	80/77.9
Si NPs optimal	21.1/19.2	1.036/1.032	23.8/22.8	85.7/80.3
Si NPs high	18.6/17.4	1.014/1.021	24.2/21.2	75.8/80.7
Si NPs extra high	17.8/16.7	1.015/0.992	22.9/22.1	76.7/76.4

Generally, these effects are correlated with our modeling and, according to Fig. S8 and Fig. 3, there is the interplay between carriers losses, changed mobility and absorption. For example, the ratio between TiO_2 and Si in the paste with the extra high Si NPs concentration is dramatically decreased meaning that TiO_2 fraction starts to be too small for efficient transport of electrons. Thus, for extra high density of Si NPs the best efficiency is lower than that for the best reference (17.8%), because of FF and V_{OC} reduction. In order to demonstrate the limit case for our approach, we prepare PSC containing Si NPs only in the mesoporous layer (i.e. without meso-TiO_2) and recorded its J–V curve (Fig. S10), revealing FF = 47.2% and V_{OC}=0.883 V. This experiment shows that there is an optimal ratio between TiO_2 and Si NPs in the mesoporous layer.

Remarkably, the PSC efficiency enhancement for the improved devices revealed from J–V curves and EQE are achieved together with their PL enhancements (Fig. S6) supporting the mechanism of light trapping by the Si NPs verified by our modeling (Fig. 3a.2,b.2,Fig. S11) and measurements on enhanced light absorption (Fig.S7). The light trapping effect almost vanishes for the case, when the distance between Si NPs is comparable or less than one TiO_2 NP in mesoporous layer (20 nm). In these cases, the sufficient part of the incident electromagnetic field can be trapped and localized between Si NPs [37], i.e., J_{SC} and V_{OC} is smaller then for a device with higher gap between Si NPs.

Regarding the hysteresis effects in PSC in the case of any additional integration of nanostructures without charge transporting function into PSC, the hysteresis influence cannot be neglected. Thus, we compared forward and reverse J–V curves recorded for the best mesoporous PSCs with different concentration of Si NPs (Fig. S12), which reveals that the measured cells have a small difference between the curves corresponding to forward and reverse scans. This is the result of high charge carriers mobility of c-Si [38] and reduction of trap states density (decrease of monomolecular constant *A* shown in Fig.S6), which are crucial parameters for strength of hysteresis [39,40].

In conclusion, we have created a mesoporous electron transport layer based on optically resonant Si NPs incorporated into TiO_2 paste and applied it for perovskite ($MAPbI_3$) solar cell improvement. The inclusion of Mie-resonant Si NPs helps to improve light absorption by a perovskite layer without reduction of the active material. The management of concentration of Si nanoantennas provide to reach a power conversion efficiency >21% by increasing of all main device parameters. The achieved level of efficiency is comparable with the record values for $MAPbI_3$-based solar cells [6,41,42]. Our multiphysical theoretical simulations of the solar cells with the resonant Si NPs provide physical understanding on the mechanisms of the device improvement as well as help to optimize the silicon nanoparticles concentration. Importantly, the optimization of ETL with Si NPs is just around 0.3% of the cost of the initial TiO_2 paste, while the increase of device's cost is even smaller. On the other hand, the average efficiency growth is larger than 1%, which indicates clear economical benefit of the proposed technology. We believe that our simple and commercially available technology can become a wide-spread tool for up-scaling high-efficient perovskite photovoltaic devices.

3. Experimental section

3.1. Chemicals and materials

FTO Pilkington (15Ω/sq), PbI_2 for perovskite preparation was used from Tokyo Chemical Industry MAI and TiO_2 paste(30 RD) from DyeSol, Chlorobenzene, Acetonitrile, DMF, DMSO, Li-TFSI, SPIRO-MeOTAD and chemicals for compact TiO_2 layer (Titanium isopropoxide, Acetylacetone and EtOH) from Sigma Aldrich, Si NPs (99.9%) with 100–200 nm in size were obtained from Getnanomaterials. To prepare a solution for compact TiO_2 1 ml of Acetylacetone was added to 1.5 ml Titanium diisopropoxide bis(acetylacetonate) and then it was properly mixed in 22.5 ml EtOH. To prepare resonant mesoporous layer commercial available Si NPs were mixed with EtOH in 1:25 mass ratio and were dispersed in ultrasonic bath to avoid agglomeration and thereafter were filtered through a 450 nm syringe filter. The TiO_2 paste was dissolved in 6 times by Si in EtOH and pure EtOH to form TiO_2-Si solutions with following proportions: (1) pure EtOH as reference samples, (2) pure Si-EtOH as extra high Si concentration to achieve the Si mass concentration in the total TiO_2 solution as 1:30, (3) Si-EtOH:pure EtOH in 1:1 as high Si concentration to achieve the Si mass concentration in the TiO_2 solution as 1:60, (4) Si-EtOH:EtOH in 1:5 as low Si concentration (the mass concentration of Si in the total solution is 1:180) and (5) Si-EtOH:EtOH in 1:3 as optimal Si concentration (1:120). 1.414 mmol $MAPbI_3$ solution dissolved in DMF:DMSO solution was used to prepare the perovskite film outside a glovebox.

3.2. Solar cell fabrication

2.5 × 2.5 cm^2 FTO glass substrates were divided by 4 individual pixels by means of a raster scanning laser (Nd:YVO_4 pulsed at 30 kHz average output power 10 W). Then the substrates were carefully cleaned by soap, DI water and i-PrOH and were exposed to the ultrasound. A 50 nm compact TiO_2 (c-TiO_2) layer was deposited onto the patterned FTO substrates by spray pyrolysis technique at 460 C and 1.5 Bar atmosphere. After that mesoporous TiO_2 solutions with resonant Si NPs in different concentrations were deposited on the c-TiO_2 layer by spin coating procedure with 3000 rpm for 20 s and then were annealed up to 480 C according to the similar procedure described in [43]. $MAPbI_3$ perovskite was deposited at room condition in the spin coater with initial 1000 rpm for 10 s and then 5000 rpm for 45 s 0.7 ml of Diethyl Ether was dropped in 38 s before the end and fresh $MAPbI_3$ layer was crystallizing at 100 C for approximately 10 min. SPIRO-MeOTAD solution in chlorobenzene doped by Li and Co salts in 10 min before deposition in glovebox. The spin regime for SPIRO-MeOTAD deposition consists one step 2000 rpm for 15 s and finally the 100 nm top gold contact layer was deposited via vacuum evaporator with 0.3 $Å/s$ for the first 10 nm and then with 1 $Å/s$ up to 100 nm thickness layer.

3.3. Characterization

Scattering by Si nanoparticles on mesoporous TiO_2 are studied be confocal dark-field optical spectroscopy. The nanoparticles are exited by linearly polarized light from a halogen lamp (AvaLight-HAL) through an objective (Mitutoyo M Plan Apo NIR, 10×, NA = 0.26)

at an oblique angle (65° with respect to the normal of the surface). Scattered light is collected from the top by a objective (Mitutoyo M Plan APO, 50×, NA = 0.55), sent to Horiba LabRam HR spectrometer, and projected onto a thermoelectrically cooled charge-coupled device (Andor DU 420A-OE 325) with a 150 g/mm diffraction grating.

Merlin (Carl Zeiss) microscope was used for SEM imaging. Mesoporous perovskite solar cell cross-section was investigated with low accelerating voltage of 1.5 kV to prevent charge effects from nonconductive substrate. In-Lens detector was chosen to get better topography resolution. Better material contrast was achieved with ESB Detector with 0.5 kV blocking voltage. Flat surface images were obtained with 5 kV accelerating voltage with working distance of 4.4 mm. Both In-lens and everhart–thornley detectors were used to gain better contrast.

Photoluminescence decay of the film was studied using time correlated photon counting technique. For these studies, PL signal was excited at 532 nm wavelength with a laser diode having the pulse duration of 100 ps and 250 kHz repetition rate, while the photon counting detector modules with a timing resolution of 50 ps was used to detect luminescence decay. The excitation signal was directed and the signal was collected by a single infinity corrected 10 times objective with NA=0.26. The excitation beam was unfocused and the laser spot had diameter approximately 160 μm.

Photoluminescence spectra were recorded on Carl Zeiss — Axio Imager. A2m microscope using an fluorescent regime and HBO 100 mercury lamp (wavelength is 375 nm) as an excitation source where PL spectra were collected by Ocean Optics spectrometer through an optical waveguide. Absorption spectra of investigated perovskite samples had been prepared via Shimadzu spectrophotometer UV-3600 Plus.

Photovoltaic performance of the devices and modules was analyzed through measurement of masked devices under a solar simulator (ABET Sun 2000, class A) at AM 1.5 G and 100 mW/cm^2 illumination conditions which was calibrated with a certified reference Si Cell (RERA Solutions RR-1002). The incident power was checked with a Skye SKS 1110 sensor. Dark JV measurement from fabricated PSCs was performed using cyclic Voltammetry module of AUTOLAB potentiostat instrument. Electrochemical impedance spectroscopy was done via AUTOLAB. TPV, TPC was measured with a commercial apparatus (Arkeo, Cicci Research s.r.l.) based on a high speed Waveform Generator that drives a high speed LED (5000 Kelvin).

XRD analysis was carried out by means of X-ray diffractometer Ultima IV Rigaku with a copper anode with λ (CuKα) = 1,5418 Å at goniometer radius of 285 mm. In the experiment, the voltage across the tube was 40 kV, the current was 40 mA, and the output power was 1.6 kW. Diffraction reflections were interpreted using the ICDD PDF-2 (2008) diffraction database.

3.4. Simulations

For calculation of optical generation rate, we used Lumerical FDTD® 2020 commercial package. Energy band diagram, net recombination rate, electron current distribution and open-circuit voltage were obtained with Lumerical CHARGE module which couples drift–diffusion and Poisson equations. The model parameters are described in details in our previous work [20]. In our 2D calculations, we consider the unit cell containing one Si NP located in TiO$_2$ layer and partially submerged in perovskite bulk. For simplicity, we replace complex morphology of the mesoporous structure by the ideal plane interface of TiO$_2$ and perovskite.

CRediT authorship contribution statement

Aleksandra Furasova: Author of the project, Experimental and measuring parts, Numerical calculations, Writing – original draft. **Pavel Voroshilov:** Data curation, Writing – original draft. **Mikhail Baranov:** SEM characterization. **Pavel Tonkaev:** Optical characterization. **Anna Nikolaeva:** Numerical calculations. **Kirill Voronin:** Numerical calculations. **Luigi Vesce:** Investigation. **Sergey Makarov:** Writing – original draft, Writing – review & editing. **Aldo Di Carlo:** Conceptualization, Data curation, Writing – original draft.

Declaration of competing interest

The authors declare that they have no known competing financial interests or personal relationships that could have appeared to influence the work reported in this paper.

Acknowledgments

Appendix A. Supplementary data

SI including SEM, XRD, optical properties, calculations and J-V data can be found at https://doi.org/10.1016/j.nanoen.2021.106484.

References

[1] Johannes M Richter, Mojtaba Abdi-Jalebi, Aditya Sadhanala, Maxim Tabachnyk, Jasmine PH Rivett, Luis M Pazos-Outón, Karl C Gödel, Michael Price, Felix Deschler, Richard H Friend, Enhancing photoluminescence yields in lead halide perovskites by photon recycling and light out-coupling, Nature Commun. 7 (1) (2016) 1–8.

[2] Sirazul Haque, Manuel J Mendes, Olalla Sanchez-Sobrado, Hugo Águas, Elvira Fortunato, Rodrigo Martins, Photonic-structured tio2 for high-efficiency, flexible and stable perovskite solar cells, Nano Energy 59 (2019) 91–101.

[3] Raphael Schmager, Guillaume Gomard, Bryce Sydney Richards, Ulrich Wilhelm Paetzold, Nanophotonic perovskite layers for enhanced current generation and mitigation of lead in perovskite solar cells, Sol. Energy Mater. Sol. Cells 192 (2019) 65–71.

[4] Qianqian Lin, Ardalan Armin, Ravi Chandra Raju Nagiri, Paul L Burn, Paul Meredith, Electro-optics of perovskite solar cells, Nat. Photon. 9 (2) (2015) 106–112.

[5] M Laska, Z Krzemińska, K Kluczyk-Korch, D Schaadt, E Popko, WA Jacak, JE Jacak, Metallization of solar cells, exciton channel of plasmon photovoltaic effect in perovskite cells, Nano Energy 75 (2020) 104751.

[6] Jinyue Du, Yuhong Zhang, Meifang Yang, Donglai Han, Lin Fan, Yingrui Sui, Jinghai Yang, Lili Yang, Fengyou Wang, Hot-carrier injection antennas with hemispherical AgO x@ Ag architecture for boosting the efficiency of perovskite solar cells, ACS Appl. Mater. Interfaces 12 (37) (2020) 41446–41453.

[7] G. Kakavelakis, K. Petridis, E. Kymakis, Recent advances in plasmonic metal and rare-earth-element upconversion nanoparticle doped perovskite solar cells, J. Mater. Chem. A 5 (41) (2017) 21604–21624.

[8] Konrad Domanski, Juan-Pablo Correa-Baena, Nicolas Mine, Mohammad Khaja Nazeeruddin, Antonio Abate, Michael Saliba, Wolfgang Tress, Anders Hagfeldt, Michaael Graztel, Not all that glitters is gold: metal-migration-induced degradation in perovskite solar cells, ACS Nano 10 (6) (2016) 6306–6314.

[9] Lusheng Liang, Yu Cai, Xin Li, Mohammad Khaja Nazeeruddin, Peng Gao, All that glitters is not gold: Recent progress of alternative counter electrodes for perovskite solar cells, Nano Energy 52 (2018) 211–238.

[10] Yuanhang Cheng, Xixia Liu, Zhiqiang Guan, Menglin Li, Zixin Zeng, Ho-Wa Li, Sai-Wing Tsang, Armin Gerhard Aberle, Fen Lin, Revealing the degradation and self-healing mechanisms in Perovskite solar cells by sub-bandgap external quantum efficiency spectroscopy, Adv. Mater. 33 (3) (2021) 2006170.

[11] Arseniy I Kuznetsov, Andrey E Miroshnichenko, Mark L Brongersma, Yuri S Kivshar, Boris Luk'yanchuk, Optically resonant dielectric nanostructures, Science 354 (6314) (2016).

[12] Boris S Luk'yanchuk, Nikolai V Voshchinnikov, Ramón Paniagua-Domínguez, Arseniy I Kuznetsov, Optimum forward light scattering by spherical and spheroidal dielectric nanoparticles with high refractive index, ACS Photon. 2 (7) (2015) 993–999.

[13] Akihiro Kojima, Kenjiro Teshima, Yasuo Shirai, Tsutomu Miyasaka, Organometal halide perovskites as visible-light sensitizers for photovoltaic cells, J. Am. Chem. Soc. 131 (17) (2009) 6050–6051.

[14] Martin A. Green, Anita Ho-Baillie, Henry J. Snaith, The emergence of perovskite solar cells, Nat. Photon. 8 (7) (2014) 506–514.

[15] Juan-Pablo Correa-Baena, Michael Saliba, Tonio Buonassisi, Michael Grätzel, Antonio Abate, Wolfgang Tress, Anders Hagfeldt, Promises and challenges of perovskite solar cells, Science 358 (6364) (2017) 739–744.

[16] Jin Young Kim, Jin-Wook Lee, Hyun Suk Jung, Hyunjung Shin, Nam-Gyu Park, High-efficiency perovskite solar cells, Chem. Rev. 120 (15) (2020) 7867–7918.

[17] Jason J Yoo, Gabkyung Seo, Matthew R Chua, Tae Gwan Park, Yongli Lu, Fabian Rotermund, Young-Ki Kim, Chan Su Moon, Nam Joong Jeon, Juan-Pablo Correa-Baena, et al., Efficient perovskite solar cells via improved carrier management, Nature 590 (7847) (2021) 587–593.

[18] Cong Chen, Shijian Zheng, Hongwei Song, Photon management to reduce energy loss in perovskite solar cells, Chem. Soc. Rev. (2021).

[19] Sergey Makarov, Aleksandra Furasova, Ekaterina Tiguntseva, Andreas Hemmetter, Alexander Berestennikov, Anatoly Pushkarev, Anvar Zakhidov, Yuri Kivshar, Halide-perovskite resonant nanophotonics, Adv. Opt. Mater. 7 (1) (2019) 1800784.

[20] Aleksandra Furasova, Pavel Voroshilov, Enrico Lamanna, Alexey Mozharov, Anton Tsypkin, Ivan Mukhin, Daniele Barettin, Konstantin Ladutenko, Anvar Zakhidov, Aldo Di Carlo, et al., Engineering the charge transport properties of resonant silicon nanoparticles in perovskite solar cells, Energy Technol. 8 (4) (2020) 1900877.

[21] Alexander Krasnok, Sergey Makarov, Mikhail Petrov, Roman Savelev, Pavel Belov, Yuri Kivshar, Towards all-dielectric metamaterials and nanophotonics, in: Metamaterials X, Vol. 9502, International Society for Optics and Photonics, 2015, 950203.

[22] Harry A. Atwater, Albert Polman, Plasmonics for improved photovoltaic devices, Mater. Sustain. Energy Collect. Peer-Rev. Res. Rev. Artic. Nat. Publish. Group (2011) 1–11.

[23] Dane W deQuilettes, Kyle Frohna, David Emin, Thomas Kirchartz, Vladimir Bulovic, David S Ginger, Samuel D Stranks, Charge-carrier recombination in halide perovskites: Focus review, Chem. Rev. 119 (20) (2019) 11007–11019.

[24] Aleksandra Furasova, Emanuele Calabró, Enrico Lamanna, Ekaterina Tiguntseva, Elena Ushakova, Eugene Ubyivovk, Vladimir Mikhailovskii, Anvar Zakhidov, Sergey Makarov, Aldo Di Carlo, Resonant silicon nanoparticles for enhanced light harvesting in halide perovskite solar cells, Adv. Opt. Mater. 6 (21) (2018) 1800576.

[25] E Tiguntseva, A Chebykin, A Ishteev, R Haroldson, B Balachandran, E Ushakova, F Komissarenko, H Wang, V Milichko, A Tsypkin, D Zuev, W Hu, S Makarov, A Zakhidov, Resonant silicon nanoparticles for enhancement of light absorption and photoluminescence from hybrid perovskite films and metasurfaces, Nanoscale 9 (34) (2017) 12486–12493.

[26] Hiroshi Sugimoto, Yusuke Ozaki, Minoru Fujii, Silicon quantum dots in dielectric scattering media: Broadband enhancement of effective absorption cross section by light trapping, ACS Appl. Mater. Interfaces 9 (22) (2017) 19135–19142.

[27] Nam-Gyu Park, Michael Grätzel, Tsutomu Miyasaka, Kai Zhu, Keith Emery, Towards stable and commercially available perovskite solar cells, Nat. Energy 1 (11) (2016) 1–8.

[28] Wolfgang Tress, Nevena Marinova, Thomas Moehl, Shaik Mohammad Zakeeruddin, Mohammad Khaja Nazeeruddin, Michael Grätzel, Understanding the rate-dependent J–V hysteresis, slow time component, and aging in CH 3 NH 3 PbI 3 perovskite solar cells: the role of a compensated electric field, Energy Environ. Sci. 8 (3) (2015) 995–1004.

[29] Nuria F Montcada, Jose Manuel Marin-Beloqui, Werther Cambarau, Jesus Jimenez-Lopez, Lydia Cabau, Kyung Taek Cho, Mohammad Khaja Nazeeruddin, Emilio Palomares, Analysis of photoinduced carrier recombination kinetics in flat and mesoporous lead perovskite solar cells, ACS Energy Lett. 2 (1) (2017) 182–187.

[30] Leyla Najafi, Babak Taheri, Beatriz Martin-Garcia, Sebastiano Bellani, Diego Di Girolamo, Antonio Agresti, Reinier Oropesa-Nunez, Sara Pescetelli, Luigi Vesce, Emanuele Calabro, et al., MoS2 quantum dot/graphene hybrids for advanced interface engineering of a CH3NH3PbI3 perovskite solar cell with an efficiency of over 20%, ACS Nano 12 (11) (2018) 10736–10754.

[31] Tao Ye, Kai Wang, Shaoyang Ma, Congcong Wu, Yuchen Hou, Dong Yang, Ke Wang, Shashank Priya, Strain-relaxed tetragonal MAPbI3 results in efficient mesoporous solar cells, Nano Energy 83 (2021) 105788.

[32] William H Nguyen, Colin D Bailie, Eva L Unger, Michael D McGehee, Enhancing the hole-conductivity of spiro-ometad without oxygen or lithium salts by using spiro (TFSI) 2 in perovskite and dye-sensitized solar cells, J. Am. Chem. Soc. 136 (31) (2014) 10996–11001.

[33] Tadeusz Bak, Maria K Nowotny, Leigh R Sheppard, Janusz Nowotny, Mobility of electronic charge carriers in titanium dioxide, J. Phys. Chem. C 112 (33) (2008) 12981–12987.

[34] Makhsud I Saidaminov, Ahmed L Abdelhady, Banavoth Murali, Erkki Alarousu, Victor M Burlakov, Wei Peng, Ibrahim Dursun, Lingfei Wang, Yao He, Giacomo Maculan, et al., High-quality bulk hybrid perovskite single crystals within minutes by inverse temperature crystallization, Nature Commun. 6 (1) (2015) 1–6.

[35] Eline M Hutter, Giles E Eperon, Samuel D Stranks, Tom J Savenije, Charge carriers in planar and meso-structured organic–inorganic perovskites: mobilities, lifetimes, and concentrations of trap states, J. Phys. Chem. Lett. 6 (15) (2015) 3082–3090.

[36] Laura M. Herz, Charge-carrier mobilities in metal halide perovskites: fundamental mechanisms and limits, ACS Energy Lett. 2 (7) (2017) 1539–1548.

[37] Reuben M Bakker, Dmitry Permyakov, Ye Feng Yu, Dmitry Markovich, Ramón Paniagua-Domínguez, Leonard Gonzaga, Anton Samusev, Yuri Kivshar, Boris Luk'yanchuk, Arseniy I Kuznetsov, Magnetic and electric hotspots with silicon nanodimers, Nano Lett. 15 (3) (2015) 2137–2142.

[38] Michael S. Shur, Handbook Series on Semiconductor Parameters, vol. 1, World Scientific, 1996.

[39] Dong-Ho Kang, Nam-Gyu Park, On the current–voltage hysteresis in perovskite solar cells: dependence on perovskite composition and methods to remove hysteresis, Adv. Mater. 31 (34) (2019) 1805214.

[40] Bo Chen, Mengjin Yang, Shashank Priya, Kai Zhu, Origin of J–V hysteresis in perovskite solar cells, J. Phys. Chem. Lett. 7 (5) (2016) 905–917.

[41] Zhaolai Chen, Bekir Turedi, Abdullah Y Alsalloum, Chen Yang, Xiaopeng Zheng, Issam Gereige, Ahmed AlSaggaf, Omar F Mohammed, Osman M Bakr, Single-crystal MAPbI3 perovskite solar cells exceeding 21% power conversion efficiency, ACS Energy Lett. 4 (6) (2019) 1258–1259.

[42] Antonio Agresti, A Pazniak, S Pescetelli, A Di Vito, D Rossi, A Pecchia, M Auf der Maur, A Liedl, R Larciprete, Denis V Kuznetsov, et al., Titanium-carbide MXenes for work function and interface engineering in perovskite solar cells, Nature Mater. 18 (11) (2019) 1228–1234.

[43] Narges Yaghoobi Nia, Enrico Lamanna, Mahmoud Zendehdel, Alessandro L Palma, Francesca Zurlo, Luigi Angelo Castriotta, Aldo Di Carlo, Doping strategy for efficient and stable triple cation hybrid perovskite solar cells and module based on poly (3-hexylthiophene) hole transport layer, Small 15 (49) (2019) 1904399.

Aleksandra Furasova is a Ph.D. student in Condensed Matter Physics in ITMO University (St. Petersburg, Russia) and in Electronic Engineering in Tor Vergata University of Rome (Italy). Her research interests have involved perovskite nanostructures, improving perovskite solar cells by resonant and nonresonant nanostructures.

Pavel Voroshilov is a PostDoc in the Laboratory of Hybrid Nanophotonics and Optoelectronics at the ITMO University. He received his M.Sc. degree in Photonics at the ITMO University (St. Petersburg, Russia) in 2014 and Ph.D. degree in Electrical Engineering at the Aalto University (Espoo, Finland) in 2018. His research interests span a broad range of topics including engineering of electromagnetic properties, light management, photovoltaics with a focus on analytical, numerical and experimental studies.

Baranov Mikhail is an engineer of ITMO University, St.Petersburg, Russia. He has been studding structures of N - doped microdiamonds. He has more than 10 years experience of SEM samples preparation and imaging. He investigates the influence of microdiamond morphology on their optical properties. He studies the penetration of nanoparticles into porous glass. Coauthor of more than 50 works in last 5 years. National and international conferences on microscopy participant.

Pavel Tonkaev received a Master of Science degree in technical physics in 2019 from ITMO University (St. Petersburg, Russia). During his M.Sc. degree, he worked on optical cooling of Mie-resonant nanoparticles. Currently, he is a Ph.D. student in ITMO University (St. Petersburg, Russia) and carries out research in the fields of nanolasers, nanophotonics, nonlinear photoluminescence and metamaterials.

Anna Nikolaeva received a Master of Science degree in technical physics in 2020 from ITMO University (St. Petersburg, Russia). During her M.Sc. degree, she worked in field of nonlinear optics, in particular, theoretical study of the processes of second harmonic generation and spontaneous parametric downconversion. She is currently a Ph.D. student at ITMO University (St. Petersburg, Russia) and is actively involved in research in the field of nanophotonics, nonlinear optics, and halide perovskites.

Kirill Voronin is a bachelor student at ITMO University (St. Petersburg, Russia). His research interests include resonant nanoparticles for photovoltaic applications.

Sergey Makarov is a professor, head of Laboratory of Hybrid Nanophotonics and Optoelectronics, dean of Faculty of Photonics, as well as director of Shared Research Facilities on Nanotechnology at the ITMO University. He received a Ph.D. degree in 2014 at the Lebedev Physical Institute of the Russian Academy of Sciences (Moscow, Russia), and Habilitated at the ITMO University (St. Petersburg, Russia). The topics of his research activity include nanophotonics, halide perovskites, laser-matter interaction, and nanotechnology.

Luigi Vesce is a researcher and of Nanoelectronics at Centre for Hybrid and Organic Solar Energy, University of Tor Vergata, where he got the Ph.D. in Telecommunications Engineering and Microelectronics in 2011. In the last years, he developed a pilot-line for a public/private consortium (Dyepower) to produce DSSC panel for BIPV. His research activity deals with the research, development, fabrication by coating/printing techniques and scaling-up of efficient and stable dye sensitized and perovskite solar technologies for outdoor and indoor applications. He is involved in national and international PV-related projects, and he is author of several contributions for international journals and conferences.

Aldo Di Carlo is a professor of Opto- and Nanoelectronics (Tor Vergata University), director of the Institute for Structure of Matter of the National Research council (CNR-ISM). His research focuses on the study and fabrication and optimization of optoelectronic devices. His research concerns the simulation of nanoelectronic systems and on scaling-technologies for industry. Di Carlo founded and direct of Center for Hybrid and Organic Solar Cells. He is the European coordinator of the H2020 project CITYSOLAR on the development of tandem cells perovskite/organics for building integration and has more than 500 publications, 13 international patents, several review papers and books.